Research on Chemical Intermediates (2019) 45:249–259
https://doi.org/10.1007/s11164-018-3600-0

Improved visible-light photoactivity of Pt/g-C_3N_4 nanosheets for solar fuel production via pretreated boric acid modification

Yuying Wang[1] · Linlu Bai[1] · Ziqing Zhang[1] · Yang Qu[1] · Liqiang Jing[1]

Received: 19 August 2018 / Accepted: 14 September 2018 / Published online: 26 September 2018

Abstract

In this work, the photocatalytic activities of g-C_3N_4 nanosheets for CO_2 conversion and H_2 production were obviously promoted by modifying an appropriate amount of Pt as the photoelectron-acceptor and co-catalyst. The optimized 0.5Pt–CN displayed $\sim$ 2-times higher photocatalytic activities for both CO_2 reduction and H_2 production than those of bare CN nanosheets. Importantly, the photocatalytic activities for solar fuel production of Pt–g-C_3N_4 nanosheets can be further enhanced by pretreating a suitable amount of boric acid modification on g-C_3N_4 nanosheets. Compared to 0.5Pt–CN and bare CN, the optimized 0.5Pt–5B–CN (5% boric acid in molar ratios) displayed $\sim$ 2- and 9-times enhancement for reducing CO_2 to CO, as well as CH_4 while $\sim$ 2- and 10-times enhancement for H_2 production, respectively. By means of the steady-state surface photovoltage spectra, fluorescence spectra and fluorescence spectra related to the produced ·OH amount, the exceptional photoactivities were comprehensively attributed to the boric acid-assisted high dispersion of Pt on g-C_3N_4 nanosheet which enhances the charge separation and improves the co-catalytic activity. This pretreated boric acid modification strategy is also applicable for other noble metals like Ag and Au. This work provides a new strategy on developing an efficient g-C_3N_4-based photocatalyst for solar fuel production.

✉ Yang Qu
quyang@hlju.edu.cn

✉ Liqiang Jing
jinglq@hlju.edu.cn

[1] Key Laboratory of Functional Inorganic Material Chemistry, Ministry of Education of the People's Republic of China, Heilongjiang University, Harbin 150080, People's Republic of China

Graphical abstract

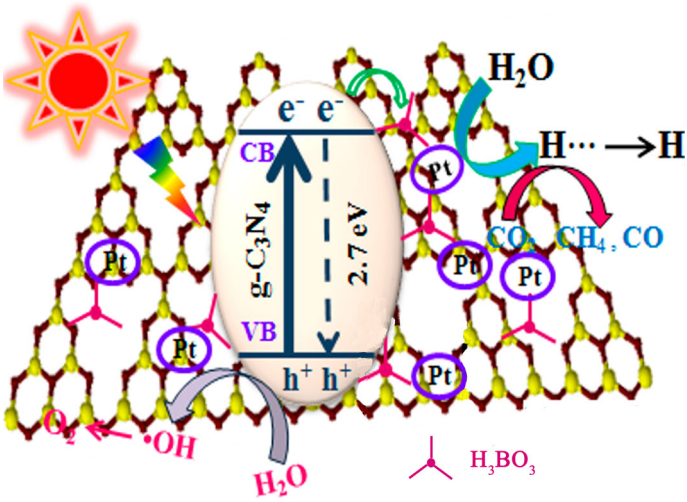

Keywords Pt/g-C_3N_4 nanosheet · Pretreated boric acid modification · Charge separation · Visible-light photocatalysis · Solar fuel production

Introduction

Because of the increasingly serious energy crisis, it is urgent to develop clean, efficient and cheap techniques to produce energy. Solar energy is an important source of an enormous amount of renewable energy, which can easily satisfy all of the energy consumption on earth [1]. In 1 h, the earth receives as much energy from the sun as humankind uses in a whole year. One way to solve the energy crisis is to transform the solar energy directly into solar fuel via photocatalysis, such as hydrogen, carbon monoxide or methane gas, from basic raw materials such as water and carbon dioxide [2–4].

Photocatalytic solar fuel production has attracted much attention in recent years because it has advantages of cleanliness and convenience [5]. Because 47% of visible light is in the solar spectrum, developing visible light response photocatalysts is meaningful [6–8]. Effective photocatalysts that can largely catalyze the process are needed to efficiently produce solar fuel, which requires rational design and synthesis of photocatalysts. Graphitic carbon nitride (g-C_3N_4 or CN) as a promising photocatalyst has received great attention in the field of sustainable energy production for CO_2 reduction and H_2 evolution, especially under visible-light irradiation, owing to its suitable energy bandgap (2.7 eV), high stability and unique surface properties [9–11]. However, the efficiency of bulk CN is still limited by its high photogenerated charge recombination rate and poor catalytic ability on the surface. To fabricate the 2D-structured CN nanosheets could enlarge the surface

area meanwhile improve the charge separation to some extent; however, this is still not enough for effective photocatalysis. Accordingly, Pt as the representative of noble metals is widely used as an effective co-catalyst for the CN catalyzed visible-light solar fuel production [12]. When Pt is loaded onto the surface of a semiconductor as the co-catalyst, the photogenerated electrons migrate to the surface of the host semiconductor and are then entrapped by Pt, since the Fermi energy level of noble metal is always lower than that of the semiconductor photocatalyst [13]. This results in the efficient separation of the photogenerated electrons and holes. Subsequently, the separately localized electrons and holes function as the reducer and oxidizer, respectively, during the photocatalytic reaction. Notably, the aggregation state of the introduced Pt as co-catalyst greatly affects the charge separation situation. It is required to avoid the over-aggregation of the noble metals on the surface of CN nanosheets. The high dispersion of noble metals decreases the distance of photogenerated electrons immigration from CN to the co-catalyst meanwhile increasing the number of catalytic sites, resulting in improved photocatalytic solar fuel production. Therefore, it is significant to achieve the high dispersion of as-introduced noble metals on the surface of CN nanosheets.

Generally speaking, an in situ photodeposition method was applied to prepare Pt loading on semiconductors as co-catalyst [14]. However, this method leads to the uncontrollable dispersion of Pt on semiconductors. Therefore, it is necessary to develop a facile and effective method to highly disperse Pt on the surface of CN nanosheets. To this end, much effort has been attempted, including surface engineering control, active group anchoring and reductive process tuning [15–17]. Previously, it was found that some OH groups modified on semiconductors can improve the dispersion of noble metals. Zheng's group has found that the OH radicals from ethylene glycol can improve the dispersion of Pd to produce single-atom Pd on TiO_2 nanosheets [18]. Thus, it is feasible to achieve the high dispersion of Pt by enriching the number of free OH groups on CN surface. In our previous works, we have found that inorganic acid modification, especially boric acid, can significantly enrich the number of OH groups on nanophotocatalysts such as TiO_2, Fe_2O_3 and g-C_3N_4 [19]. Therefore, it is feasible to modify CN nanosheets with boric acid to enrich the number of OH groups so as to realize the high dispersion of Pt [20, 21]. However, there are few works focusing on boric acid modification to improve the dispersion of Pt on g-C_3N_4 for photocatalysis.

Hence, Pt with different amounts were modified on g-C_3N_4 nanosheets through a wet chemical method. By examining the photocatalytic activities for visible-light H_2 production, the loading amount of Pt was optimized and corresponding sample was noted as 0.5Pt–CN. The optimized 0.5Pt–CN exhibited the highest photoactivity. On the contrast, 0.5 wt% Pt was loaded on boric acid pretreated CN nanosheets with distinct concentration. Compared to bare CN nanosheets and 0.5Pt–CN, the optimized 0.5Pt–5B–CN displays $\sim$ 2- and 9-time enhancement for CO_2 reduction, as well as $\sim$ 2- and 10-times enhancement for H_2 production, respectively. This significant enhancement is attributed to the greatly improved dispersion of Pt on g-C_3N_4 nanosheet due to the modified boric acid, resulting in the enhanced charge separation and improved the catalytic capacity. This method is also versatile to some other noble metals like Au and Ag. This work has proposed a new strategy for

preparing high dispersion noble metals on semiconductors by boric acid modification. It refers to the design and synthesis of high activity nanophotocatalysts for solar fuel production.

Experimental

All the reagents including urea, $H_2PtCl_6{\cdot}6H_2O$, boric acid and absolute ethanol were of analytical grade and used as-received without further purification. Deionized H_2O was used throughout the experiments.

Synthesis of g-C_3N_4 nanosheet (CN)

CN was obtained simply by the calcination of urea. In a typical experiment, 35 g of urea was taken in a ceramic crucible and heated in a muffle furnace at 550 °C (1 °C min^{-1} in N_2) for 3 h. After that, the obtained CN was milled by mortar to make the caked particles very small.

Synthesis of *m*Pt-CN

Two grams of the as-obtained CN was dispersed in 150 mL deionized H_2O with vigorous stirring in a 200-mL round-bottom flask. A certain volume of aqueous $H_2PtCl_6{\cdot}6H_2O$ solution was then added into the CN suspension drop by drop. The aqueous suspension was stirred (300 rpm) in 80 °C water bath in the dark for 1 h. Finally, the product was centrifuged, washed with absolute ethanol repeatedly, and dried at 80 °C. The samples were represented by *m*Pt–CN, in which m means the weight ratios of Pt to CN.

Synthesis of 0.5Pt–*X*B–CN

One gram of as-fabricated CN was dispersed in 20 mL deionized H_2O with vigorous stirring (450 rpm) in a 60 mL round bottom flask. Different amounts of boric acid with the molar ratios of 2, 5 and 8%, respectively, was added and ultrasonically treated for 30 min. Subsequently, the resulting aqueous suspension was transferred into a stainless-steel vessel and kept at 120 °C for 2 h. After cooling to room temperature naturally, the product was centrifuged, washed with absolute ethanol, and then dried at 80 °C. Finally, (0.5 wt%) Pt was loaded on the boric acid modified CN by the same method above. The samples were represented by 0.5Pt–*X*B–CN, in which *X*% means different molar ratios between boric acid and CN.

The synthesis of 0.5Au–*X*B–CN and 0.5Ag–*X*B–CN follows the same procedure except using $HAuCl_4$ and $AgNO_3$ as raw material.

Characterization

X-ray powder diffraction (XRD) measurements of the samples were carried out with an XRD Bruker D8 instrument (Germany), using Cu Kα radiation

(α = 0.15418 nm), at an accelerating voltage of 30 kV and an emission current of 20 mA was employed. Electron micrographs were taken on a JEOL JEM-2100 transmission electron microscope (TEM) operated at 200 kV. The UV–Vis diffuse reflectance spectra (DRS) were recorded with a Shimadzu UV-2550 spectrometer. The photoluminescence (PL) spectra of the samples were measured with a Perkin-Elmer LS 55 spectrofluoro-photometer at excitation wavelength of 390 nm. The atmosphere-controlled steady-state surface photovoltage spectroscopy (SS-SPS) measurements of the samples were carried out with a home-built apparatus, equipped with a lock-in amplifier (SR830) synchronized with a light chopper (SR540). The powder sample was sandwiched between two indium-tin-oxide (ITO) glass electrodes kept in an atmosphere-controlled sealed container. A monochromatic light was obtained from 500 W xenon lamp (CHF XQ500W, Global xenon lamp power) through a double prism monochromator (SBP300).

Evaluation of produced ·OH amount

To measure the ·OH amount, coumarin trapping fluorescent method was used in which coumarin reacts with ·OH radicals to produce 7-hydroxy coumarin to burst fluorescence at approximately 460 nm in photoluminescence spectrum. A 0.05 g amount of each sample powder was dispersed in 40 mL of 0.001 M coumarin aqueous solution contained in a quartz reactor. Prior to irradiation, the reactor was magnetically stirred (300 rpm) for 30 min to attain an adsorption–desorption equilibrium. After irradiation for 1 h, the sample was centrifuged and a certain amount was transferred into a Pyrex glass cell for the fluorescence measurement of 7-hydroxycoumarin at 390 nm excitation wavelength and emission wavelength at 460 nm through a spectrofluorometer (Perkin-Elmer LS 55).

Photocatalytic hydrogen production

The photocatalytic hydrogen evolution was carried out in an online hydrogen production system (Perfectlight, Beijing, LabSolar II). Eighty milliliters of deionized water and 20 mL methanol were mixed in the cubic glass cell and keep stirring at 400 rpm. Then, 0.1 g of photocatalyst powder was put into the solution. Ahead of the reaction, the mixture was deaerated by evacuation to remove the gas dissolved in water. The experiments were performed by illuminating the mixture solution, using a xenon lamp (300 W) with a 420 CUT filter (420–780 nm) as the visible light source. The amount of evolved H_2 in the photocatalysis process were performed in an inline gas chromatograph (7900, TCD, molecular sieve 5 Å, N_2 carrier, Techcomp).

Evaluation of photocatalytic activities for CO_2 conversion

In the photocatalytic conversion of CO_2, for each experiment, 0.2 g powder sample was dispersed in H_2O (3 mL) contained in a cylindrical steel reactor with a volume of 100 mL and an area of 3.5 cm^2. A 300 W xenon arc lamp was used as the light source with a cut-off filter ($\lambda \geq 420$ nm) for the photocatalytic reaction. High purity

CO_2 gas was passed through H_2O and then entered into the reaction setup for reaching ambient pressure. The used photocatalyst was allowed to equilibrate in the CO_2/H_2O system for 1 h. During irradiation, 0.5 mL gas was continually taken from the reaction cell at given time interval for the analyses of CO and O_2 concentration with the help of a gas chromatograph (Tech, GC-7900 with TCD by N_2 gas carrier). Similarly, the amount of CH_4 was detected with FID (GC-2014 with Shimadzu Corp., Japan, with N_2 gas carrier).

Results and discussion

The amount of Pt loading on g-C_3N_4 is much important for photocatalytic solar fuel production because over-loading leads to aggregation, which is harmful to the activity. In order to confirm the optimal amount of Pt loading, different amounts of Pt were loaded on g-C_3N_4 nanosheets. As shown in Fig. 1, one can see that the photocatalytic activities of g-C_3N_4 for H_2 production are highly improved after modifying Pt. The sample 0.5Pt–CN showed the highest activity for photocatalytic hydrogen production due to the appropriate amount of Pt loading. Thus, the following experiment the Pt loading amount kept this loading amount.

XRD and UV-DRS are typical techniques to study the crystal structure and optical property of nanomaterials [22, 23]. The XRD patterns of bulk CN, 0.5Pt–CN and 0.5Pt–*X*B–CN (*X* = 2, 5 and 8) are shown in Fig. 2a. One can see that there is an obvious diffraction peak in all the samples at $2\theta = 27.4°$, which is attributed to the (002) plane of graphitic carbon [24]. It is noticed from the XRD patterns of Pt loaded and boric acid modified catalysts that the characteristic diffraction peaks of Pt and boric acid are not detected, which may be attributed to the very low amount. To investigate the optical behavior of the samples, UV–Vis DRS spectra were recorded. From Fig. 2b, it can be seen that the thresholds of DRS spectra of the CN based samples are about at 460 nm, corresponding to the energy bandgap of 2.7 eV.

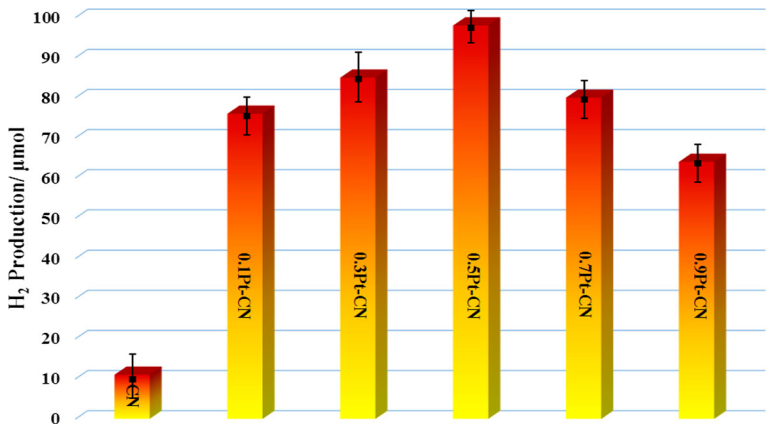

Fig. 1 Photocatalytic activities for hydrogen production over Pt loaded g-C_3N_4 nanosheets with different amounts under visible light irradiation for 1 h. Error bar: 5%

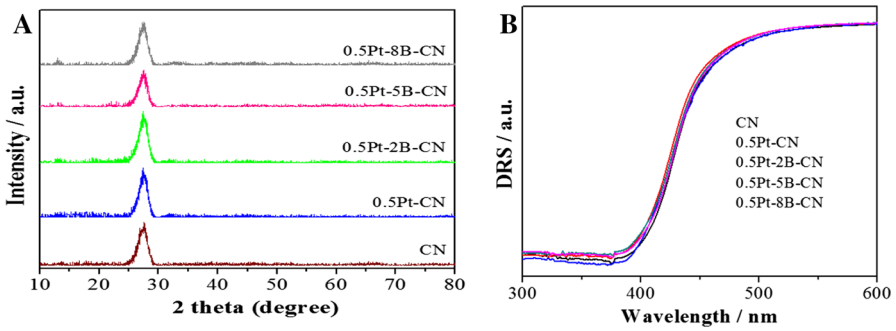

Fig. 2 XRD patterns (**a**) and UV-DRS (**b**) of CN, 0.5Pt–CN and 0.5Pt–*X*B–CN (*X* = 2, 5 and 8)

This demonstrates that the optical absorption is nearly unchanged after decorating Pt and co-modifying Pt and boric acid. This is in consistent with the results of XRD, attributed to the low loading. In this work, TEM and HRTEM were tried to show the improved dispersion of Pt on CN nanosheets via pretreated boric acid. However, it failed to directly observe the loaded Pt and modified boric acid from TEM and HRTEM images, which may due to the low amount and good dispersion. According to atomic absorption spectrometry (AAS, Thermo Elemental SOLAAR-M, limit of identification: 5 μg L^{-1}), the content of Pt in 0.5Pt–5B–CN is only 0.03%. Obviously, it is lower than the limitation of TEM and XPS.

The visible-light activities of CN, 0.5Pt–CN and 0.5Pt–*X*B–CN (*X* = 2, 5 and 8) were evaluated for CO_2 reduction with H_2O as the reducing agent. As shown in Fig. 3a, compared with bulk CN and 0.5Pt–CN, the co-catalyst free photocatalytic activities of boric acid modified 0.5Pt–CN samples for CO_2 conversion under the visible light irradiation were remarkably enhanced. The photoactivity was promoted along with the increasing amount of boric acid. However, the over amount of boric acid modification is unfavourable to improve the activity, which may be ascribed to the molecular association of boric acid molecules [20, 25]. The production rate of CO and CH_4 are 4.5 and 1.8 μmol h^{-1} g^{-1}, respectively, for the optimized 0.5Pt–5B–CN sample. Meanwhile, O_2 as the oxidative product of water is found to be

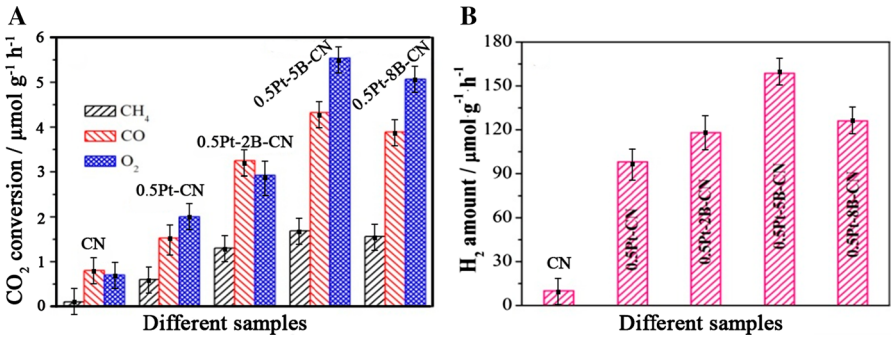

Fig. 3 Photocatalytic activities for CO_2 reduction (**a**) and H_2 production (**b**) over CN, 0.5Pt–CN and 0.5Pt–*X*B–CN (*X* = 2, 5 and 8) under visible light irradiation. Error bar: 5%

5.5 μmol h^{-1} g^{-1} for 0.5Pt–5B–CN, which coincides the balance of positive charge (four holes would be consumed to produce one O_2 molecule) and negative charge (two electrons would be consumed to produce one CO molecule and eight electrons would be consumed to produce one CH_4 molecule). Remarkably, the visible-light activity of CO_2 reduction for 0.5Pt–5B–CN exhibited nearly 9-times and 2-times enhancement as compared to those of bulk CN and 0.5Pt–CN, respectively. In addition, as for photocatalytic hydrogen production, the boric acid modified ones also exhibited promoted photoactivities (Fig. 3b). The produced H_2 gas over the optimized 0.5Pt–5B–CN sample is up to 165 μmol h^{-1} g^{-1}, which is 10-times and 2-times higher than those of bulk CN and 0.5Pt–CN, respectively.

Exploring the photogenerated charge carrier properties of semiconductor solid materials in photocatalysis, particularly for nanosized semiconductors with the negligible built-in electric field is a great challenge, but very meaningful to the photocatalysis. Steady-state surface photovoltage spectroscopy (SS-SPS) as a highly sensitive and direct method is applied to investigate the charge separation [26, 27]. Generally speaking, according to the fundamental principle of SS-SPS, the strong SS-SPS response frequently corresponds to the high photogenerated charge separation for nanomaterials [28]. Based on the response range and the bandgap energy of CN, it is claimed that the SS-SPS responses result from the band–band electron transitions. In Fig. 4a, the SS-SPS response of 0.5Pt–CN and 0.5Pt–*X*B–CN is higher than that of CN, especially that modified by boric acid, indicating the positive effect of Pt loading and boric acid modification on CN. 0.5Pt–5B–CN displays the highest SPS response, implying the best charge separation, which is in accordance with the photocatalytic activity. In addition, the decreased PL signals after the modification with Pt and boric acid, as is shown in the inset of Fig. 4a, further supports the SS-SPS results on the photophysics.

Produced hydroxyl radicals (·OH) during the photocatalytic reaction is related to the separated charge, which can reflect the charge separation in photochemistry. To further investigate the charge separation, coumarin fluorescent method was used to detect the amount of ·OH, in which the coumarin reacts with ·OH to produce luminescent 7-hydroxycoumarin [29]. It is generally accepted that the stronger is the

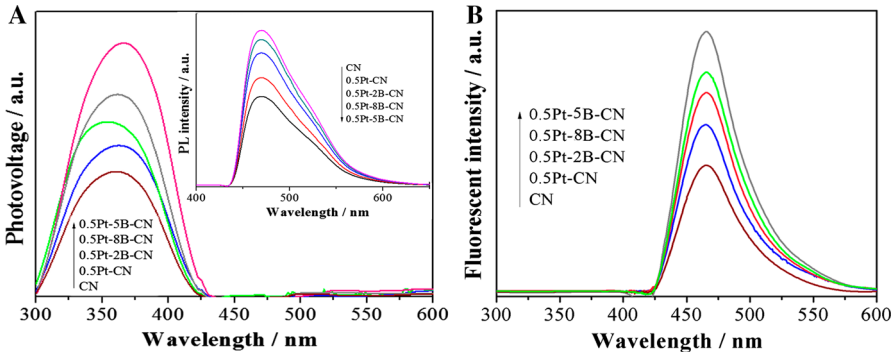

Fig. 4 SS-SPS responses (**a**), PL spectra (inset a) and ·OH radical amount-related fluorescence spectra (**b**) of CN, 0.5Pt–CN and 0.5Pt–*X*B–CN (*X* = 2, 5 and 8)

fluorescent signal, the larger is the produced ·OH amount. The amounts of produced ·OH for CN, 0.5Pt–CN and 0.5Pt–*X*B–CN samples are shown in Fig. 4b. It is clear that the amount of produced ·OH on 0.5Pt–CN is larger than that on CN, and its amount is considerably increased after decorating boric acid. Interestingly, the largest amount of produced ·OH is detected for the 0.5Pt–5B–CN nanocomposite, which further proves the enhanced charge separation of CN by loading Pt on boric acid pretreated CN.

Furthermore, this boric acid pretreating strategy can be extended to other noble metals such as Au and Ag to increase their dispersion so as to promote the photocatalytic activity. As shown in Fig. 5a, there is unchanged in both the crystal structure and optical properties for 0.5M–5B–CN samples when Au or Ag are loaded, compared with bulk CN.

Similar to Pt loading, both Au and Ag loading can also enhance the charge separation of CN to a certain degree. The PL spectra in Fig. 5b further confirm this rule, through the decreased PL signals. Moreover, there is an enhanced charge separation of CN after loading different noble metals and the rules are further verified by the produced ·OH radicals, as it is shown in Fig. 5c. In general, the enhanced charge separation leads to the promoted photocatalytic activities. The photocatalytic activities of different samples in Fig. 5d show the consistent rules of

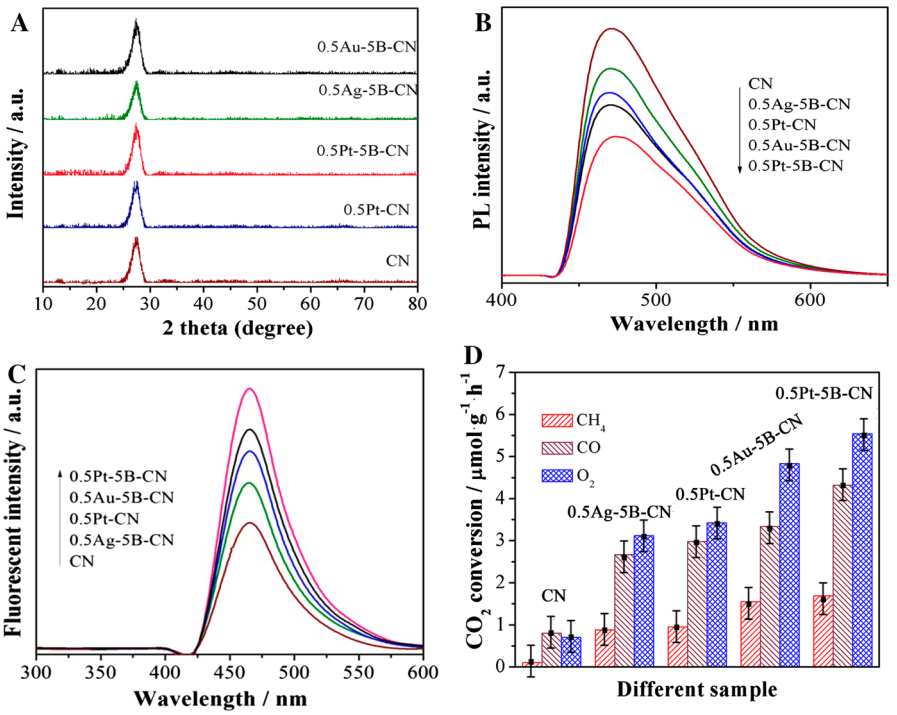

Fig. 5 XRD patterns (**a**), PL spectra (**b**), ·OH radical amount-related fluorescence spectra (**c**) and photocatalytic activities for CO_2 reduction (**d**) of CN, 0.5Pt–CN and 0.5M–5B–CN (M = Ag, Au and Pt). Error bar: 5%

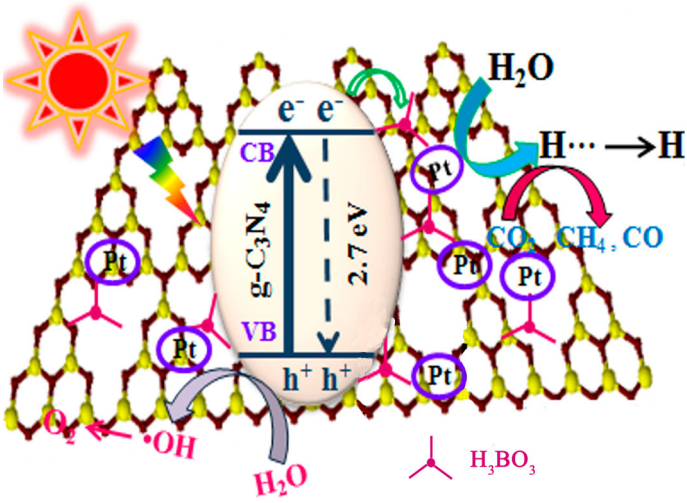

Fig. 6 Mechanism of the enhanced charge separation by 0.5Pt–5B–CN

the charge separation. 0.5Pt–5B–CN sample displays the highest activity for CO_2 reduction, which is higher than that of 0.5Au–5B–CN and 0.5Ag–5B–CN sample.

Based on these results, it is demonstrated that boric acid modification is available to improve the dispersion of Pt on CN, resulting in the enhanced charge separation and the consequently promoted photocatalytic activities for solar fuel production. A schematic is drawn to illustrate this, which is shown in Fig. 6. The modified boric acid with OH groups causes uniform Pt growth on the surface of CN, and the boric acid molecules can also act as electron acceptors to drive the charge separation. In addition, the excellent catalytic capacity of Pt accelerates the co-catalytic function to the photocatalytic solar fuel production.

Conclusions

In summary, the photocatalytic activity for solar fuel production of CN nanosheets is promoted by modifying a suitable amount of Pt by wet chemical method due to the excellent co-catalytic capacity. Furthermore, the dispersion of Pt has been successfully improved by pretreating boric acid on CN nanosheets. By means of SS-SPS, PL and produced ·OH radicals, it is confirmed that the charge separation of CN is enhanced by improving the dispersion of Pt, leading to high photocatalytic activity. The amount optimized 0.5Pt–5B–CN sample displayed outstanding photocatalytic activity for converting CO_2 to CO (4.5 μmol h^{-1} g^{-1}) and CH_4 (1.8 μmol h^{-1} g^{-1}), and producing H_2 gas (165 μmol h^{-1} g^{-1}). It is about 9-times higher for CO_2 reduction and 10-times higher for H_2 production, compared to bulk CN. This boric acid pretreated method is also versatile to other noble metals such as Ag and Au. This work shows a facile method to improve the dispersion of noble

metals on nanophotocatalysts to improve the photocatalytic activity as much as possible.

Acknowledgements This work was supported by the National Natural Science Foundation of China (U1401245, 21706044, 21501052 and 91622119), the China Postdoctoral Science Foundation (2015M570304, 2017M621316) and Special Funding for Postdoctoral of Heilongjiang Province (LBH-TZ0619).

References

1. S.J.A. Moniz, S.A. Shevlin, D.J. Martin, Z.X. Guo, J.W. Tang, Energy Environ. Sci. **8**, 731 (2015)
2. A.A. Farghali, W.M.A.E. Rouby, A. Hamdedein, Res. Chem. Intermed. **43**, 7171 (2017)
3. H. Dong, X. Guo, Y. Yin, Res. Chem. Intermed. **44**, 3151 (2018)
4. J. Zhang, H. Xu, H. Chen, M. Anpo, Res. Chem. Intermed. **196**, 232 (2016)
5. Z.Y. Wang, S. Yan, Y.J. Sun, T. Xiong, F. Dong, W. Zhang, Appl. Catal. B Environ. **29**, 839 (2003)
6. N.S. Shaha, J.A. Khan, M. Sayed, Z.U.H. Khan, A.D. Rizwan, N. Muhammad, G. Boczkaj, B. Murtaza, M. Imran, H.M. Khan, G. Zaman, Chem. Eng. J. **351**, 841 (2018)
7. M. Sayed, J.A. Khan, L.A. Shah, N.S. Shaha, F. Shah, H.M. Khan, P. Zhang, H. Arandiyan, J. Phys. Chem. C **122**, 406 (2018)
8. M. Sayed, L.A. Shah, J.A. Khan, N.S. Shah, J. Nisar, H.M. Khan, P. Zhang, A.R. Khan, J. Phys. Chem. A **120**, 9916 (2016)
9. K. Li, Z. Zeng, L. Yan, M. Huo, Y. Guo, S. Luo, X. Luo, Appl. Catal. B Environ. **187**, 269 (2016)
10. J. Zhang, Y. Chen, X. Wang, Energy Environ. Sci. **8**, 3092 (2015)
11. W.J. Ong, L.L. Tan, Y.H. Ng, S.T. Yong, S.P. Chai, Chem. Rev. **116**, 7159 (2016)
12. Y. Qu, W. Zhou, Y. Xie, L. Jiang, J. Wang, G. Tian, Z. Ren, C. Tian, H.G. Fu, Chem. Commun. **49**, 8510 (2013)
13. J. Ran, J. Zhang, J. Yu, M. Jaroniec, S.Z. Qiao, Chem. Soc. Rev. **43**, 7787 (2014)
14. X. Chen, S. Shen, L. Guo, S.S. Mao, Chem. Rev. **110**, 6503 (2010)
15. F. Fina, H. Ménard, J.T.S. Irvine, Chem. Chem. Phys. **17**, 13929 (2015)
16. T. Tong, B.C. Zhu, C.J. Jiang, B. Cheng, JGYu. Appl, Surf. Sci. **433**, 1175 (2018)
17. F. Sun, S. Tan, H. Zhang, Z. Xing, R. Yang, B. Mei, Z. Jiang, J. Colloid Interface Sci. **531**, 119 (2017)
18. P. Liu, Y. Zhao, R. Qin, S. Mo, G. Chen, L. Gu, D.M. Chevrier, P. Zhang, Q. Guo, D. Zang, B. Wu, G. Fu, N. Zheng, Science **352**, 797 (2016)
19. Z. Li, Y. Luan, Y. Qu, L. Jing, ACS Appl. Mater. Interfaces **7**, 22727 (2015)
20. C. Li, F. Raziq, C. Liu, Z. Li, L. Sun, L. Jing, Appl. Surf. Sci. **358**, 240 (2015)
21. P. Luan, M. Xie, X. Fu, Y. Qu, X. Sun, L. Jing, Phys. Chem. Chem. Phys. **17**, 5043 (2015)
22. W. Subramonian, T.Y. Wu, S.-P. Chai, J. Alloys Compd. **695**, 496 (2017)
23. C.Y. Teh, T.Y. Wu, J.C. Juan, Catal. Today **256**, 365 (2015)
24. Z. Sun, H. Wang, Z. Wu, L. Wang, Catal. Today **300**, 160 (2018)
25. A. Zaleska, E. Grabowska, J.W. Sobczak, M. Gazda, J. Hupka, Appl. Catal. B Environ. **89**, 469 (2009)
26. J. Shan, F. Raziq, M. Humayun, W. Zhou, Y. Qu, G. Wang, Y. Li, Appl. Catal. B Environ. **219**, 10 (2017)
27. L. Li, P.A. Salvador, G.S. Rohrer, Nanoscale **6**, 24 (2014)
28. S. Chen, R. Yan, X. Zhang, K. Hu, Z. Li, M. Humayun, Y. Qu, L. Jing, Appl. Catal. B Environ. **209**, 320 (2017)
29. C. Chen, W. Ma, J. Zhao, Chem. Soc. Rev. **39**, 4206 (2010)